

LA-UR-19-28017 (Accepted Manuscript)

## Studies of reactive and nonreactive metals–ejecta–transporting nonreactive and reactive gases and vacuum

Buttler, William Tillman; Cooley, Jason Christopher; Hammerberg, James Edward; Schulze, Roland K.; Schwarzkopf, John Dennis; Sheppard, Daniel Glen; Barefield, James E.; Charonko, John James; Goett, John Jerome III; Manzanares, Ruben; Martinez, John Israel; Schauer, Martin Michael; Schmidt, Derek William; Grover, Michael; La Lone, Brandon M.; Mance, Jason G.; Stevens, Gerald D.; Turley, William D.; Valencia, Robert J.

Provided by the author(s) and the Los Alamos National Laboratory (2020-12-18).

**To be published in:**

**DOI to publisher's version:** 10.1063/12.0000890

**Permalink to record:** <http://permalink.lanl.gov/object/view?what=info:lanl-repo/lareport/LA-UR-19-28017>

**Disclaimer:**

Los Alamos National Laboratory, an affirmative action/equal opportunity employer, is operated by Triad National Security, LLC for the National Nuclear Security Administration of U.S. Department of Energy under contract 89233218CNA00001. By approving this article, the publisher recognizes that the U.S. Government retains nonexclusive, royalty-free license to publish or reproduce the published form of this contribution, or to allow others to do so, for U.S. Government purposes. Los Alamos National Laboratory requests that the publisher identify this article as work performed under the auspices of the U.S. Department of Energy. Los Alamos National Laboratory strongly supports academic freedom and a researcher's right to publish; as an institution, however, the Laboratory does not endorse the viewpoint of a publication or guarantee its technical correctness.

# Studies of reactive and nonreactive metals–ejecta–transporting nonreactive and reactive gases and vacuum

Cite as: AIP Conference Proceedings **2272**, 120003 (2020); <https://doi.org/10.1063/12.0000890>  
Published Online: 04 November 2020

W. T. Buttler, J. C. Cooley, J. E. Hammerberg, R. K. Schulze, J. D. Schwarzkopf, D. G. Sheppard, J. E. Barefield, J. J. Charonko, J. J. Goett, M. Grover, B. M. La Lone, J. G. Mance, R. Manzanares, J. I. Martinez, M. M. Schauer, D. W. Schmidt, G. D. Stevens, W. D. Turley, and R. J. Valencia



[View Online](#)



[Export Citation](#)

Meet the Next Generation  
of Quantum Analyzers

And Join the Launch  
Event on November 17th



[Register now](#)



Zurich  
Instruments



# Studies of Reactive and Nonreactive Metals–Ejecta–Transporting Nonreactive and Reactive Gases and Vacuum

W. T. Buttler,<sup>1, a)</sup> J. C. Cooley,<sup>1</sup> J. E. Hammerberg,<sup>1</sup> R. K. Schulze,<sup>1</sup> J. D. Schwarzkopf,<sup>1</sup> D. G. Sheppard,<sup>1</sup> J. E. Barefield,<sup>1</sup> J. J. Charonko,<sup>1</sup> J. J. Goett III,<sup>1</sup> M. Grover,<sup>2</sup> B. M. La Lone,<sup>2</sup> J. G. Mance,<sup>2</sup> R. Manzanares,<sup>1</sup> J. I. Martinez,<sup>1</sup> M. M. Schauer,<sup>1</sup> D. W. Schmidt,<sup>1</sup> G. D. Stevens,<sup>2</sup> W. D. Turley,<sup>2</sup> and R. J. Valencia<sup>2</sup>

<sup>1)</sup>Los Alamos National Laboratory, Los Alamos, NM, 87545 USA

<sup>2)</sup>Mission Support and Technical Services, Santa Barbara, CA, 93111 USA

<sup>a)</sup>Corresponding author: [buttler@lanl.gov](mailto:buttler@lanl.gov)

**Abstract.** We report recent results of reactive and nonreactive metal fragments–ejecta–transporting in vacuum, and reactive and nonreactive gases. We postulate that reactive ejecta transporting in a reactive gas, such as D<sub>2</sub>, will rapidly break up into smaller fragments in situations where they are otherwise hydrodynamically stable in a nonreactive gas such as He. The ejecta were formed through explosive loading of thin Sn (nonreactive) and Ce (reactive) coupons that included machined periodic perturbations on their backsides, which interfaced with vacuum, He or D<sub>2</sub>. Coupon surface hydrodynamics, ejecta mass- and size-velocity distributions, and ejecta temperatures were diagnosed with laser doppler velocimetry, piezoelectric transducers, Mie scattering and infrared imaging (IR). In addition, particle imaging velocimetry was applied for the first time to evaluate ejecta transport to study ejecta sheet breakup dynamics. The IR data demonstrate that rapid reactions of Ce ejecta transporting in D<sub>2</sub> occur.

## INTRODUCTION

The results presented here follow from a 2016 research proposal submitted to the Los Alamos National Laboratory *Laboratory Directed Research & Development Directed Research (DR)* program [1]. The DR centers on the hypothesis that *reactive Ce fragments ejected into D<sub>2</sub> will react rapidly and breakup into smaller fragments in situations where they are otherwise hydrodynamically stable in a non-reactive gas such as He*. The hypothesis is validated by observation of (1) rapid heating of Ce ejecta due to  $\text{Ce} + \text{D}_2 \mapsto \text{CeD}_2 - \Delta H$  exothermic reactions, where the heat of formation  $\Delta H = 205$  kJ/mol, and (2) the rapid breakup of hydrided ejecta into submicron particles.

Initial results from this research are reported in [2], where we studied Ce cast by ESPI Metals. Also developed in [2] are initial approaches to estimate the fractional conversion of Ce ejecta to CeD<sub>2</sub>. Since then we have developed our conversion models further, as found in these SCCM-19 conference proceedings [3].

Subsequent to the initial experiments, one of us has made the cold rolled Ce (0.9995 purity) that we use in our experiments. We have also improved our target and gas handling techniques, improved our experimental packages (see Fig. 1), and fielded about 70 high explosive (HE) driven experiments on Sn and Ce coupons. The back-sides of the Sn and Ce coupons included periodic perturbations to eject Sn and Ce fragments into vacuum or the He and D<sub>2</sub> gases. The majority of the data from the HE experiments compares nonreactive ejecta from Sn with reactive ejecta from Ce transporting in reactive- and nonreactive-gases to understand reactive ejecta transport processes.

We apply a number of well developed diagnostics to differentiate reactive- and nonreactive-ejecta transport phenomena. For example, we apply laser doppler velocimetry (LDV) [4-9], Mie scattering [10-13], lithium niobate piezoelectric transducers (LN-pins) [14, 15] and infrared (IR) imaging to diagnose experimental hydrodynamics, size- and mass-velocity distributions, and ejecta radiance temperatures in vacuum and gases. And, we apply other well developed diagnostics to shock physics geometries for the first time, i.e., Coherent anti-Stokes Raman Scattering spectroscopy (CARS) and particle imaging velocimetry (PIV) to measure post-shock gas temperatures and document ejecta-sheet breakup dynamics.

To support the comparisons we developed a thermal model that explains asymptotic temperatures for Sn transporting in He and D<sub>2</sub>, and for Ce transporting in He. In these three nonreactive transport situations, we calculate the shock heated and compressed gas temperatures with the piston approximation and the ideal gas law, as well as with hydrodynamic simulations of our explosive, metal coupon and gas package geometries. In the reactive cases of Ce transporting in D<sub>2</sub>, we observe heating that can only be explained by reactions of Ce ejecta with D<sub>2</sub>, given that we see no emissions of He, D<sub>2</sub>, Sn or Ce on any other experiment. Therefore, without question CeD<sub>2</sub> forms, and that formation is accompanied by a release of heat–blackbody radiation. We are observing heat, not atomic transitions.

## EXPERIMENTAL DETAILS AND INITIAL RESULTS

Because our approaches for diagnosing surface hydrodynamics, ejecta masses and sizes, and the imaging of ejecta are extensively reported [15-23], we do not discuss most of those details here. However, some of our experiments reported here included CARS and PIV diagnostics fielded for the first time in HE geometries, and we thus provide some elaboration.

Our first HE driven (DR) Ce experiments were fielded with a single, cylindrical PBX 9501 pellet to explosively shock 3 mm tall and 50 mm diameter Ce targets (our PBX 9501 pellets are 12.7 mm diameter cylinders that are 12.7 mm tall, and two pellets are 25.4 mm tall). Prior to that work we simulated the HE- and coupon-geometries with the published Ce equation of state (EOS) [24], which in tabulated form is known as SESAME 90600 [25]. Our simulations, SESAME 90600 implied that HE driven Ce with jump velocities of  $u_j = 1.95 \text{ mm}/\mu\text{s}$ , which is a shockwave loading pressure of  $P_L \approx 19 \text{ GPa}$  that would leave the Ce in liquid state post shock and release. However, we concluded from the Mie scattering [26], LDV and LN-pin data results in this pellet and coupon geometry that the Ce ejecta were solid post shock. Subsequently, we modified our drive to include 2 PBX 9501 pellets and we thinned the Ce to 1.75 mm. Based on private communications, our current understanding is that the Ce will be liquid post shock and release with  $u_j \approx 2.35 \text{ mm}/\mu\text{s}$  and  $P_L \approx 25 \text{ GPa}$ . Initial hydrotests imply the Ce ejecta are melted in this geometry, which we are now fielding.

### Target Finishes

Our target finishes were chosen such that the fastest ejecta would be slower than the shockwave in the diatomic  $\text{D}_2$  gas. The shockwave in monatomic He is faster than that of diatomic  $\text{D}_2$ , and it meant that our wavenumber ( $k = 2\pi/\lambda$ , where  $\lambda$  is the perturbation wavelength) amplitude ( $h_0$ ) products were nominally  $kh_0 = 0.25$  for Sn, and  $kh_0 = 0.35$  for Ce. These differences account for the different shock velocities in Sn versus Ce at the shockwave loading pressures  $P_i$ .

The backsides of our targets were either diamond turned (DT, or mirror like) for CARS, fly-cut with the cutting tool positioned on a bar at a radius of 150 mm for IR and ejecta, or a large radius “up” finish. The up-finish includes a strip of periodic perturbations elevated above a flat, DT region of the target; DT finishes suppress ejecta formation to reveal the dynamics of periodic Richtmyer-Meshkov (RM) unstable sheet behavior.

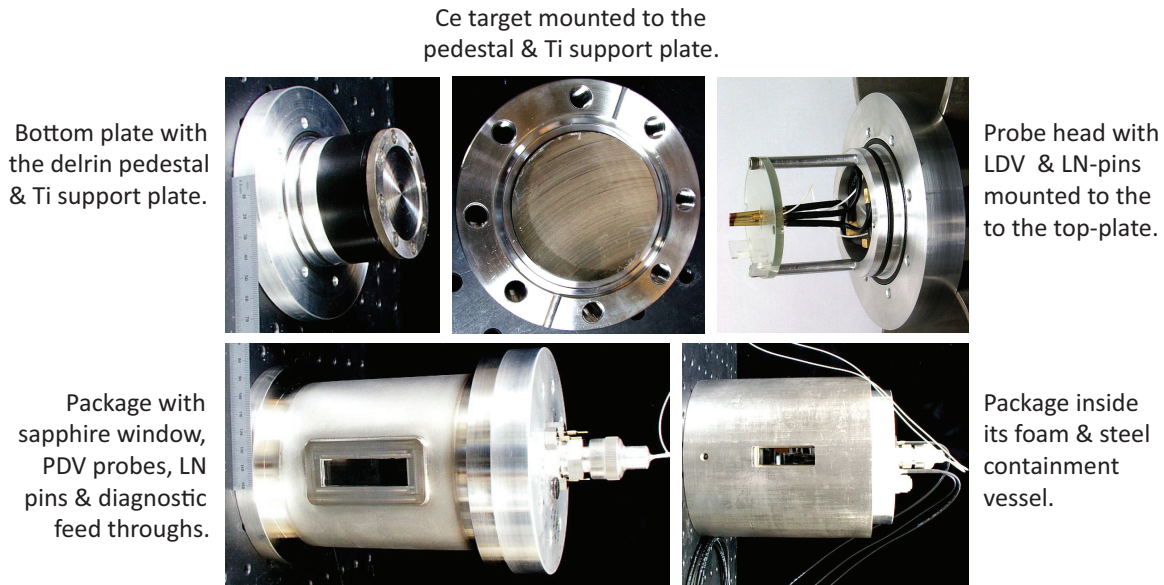


**FIGURE 1.** Ce and Sn experimental packages. HE inserts from the left into the delrin, and the packages accommodate initial pressures from 0.1- to 7000-torr.

The up-finish can be contrasted with the “down” finish we have previously fielded on Mie scattering experiments, e.g., see Fig. 6 in [11]. The difference between the up- and down-finish is that the down-finish periodic perturbations are *below* the flat DT region. These up- and down-finishes present different problems.

In the case of the down-finish, the faceted interface at the DT-perturbation intersection causes a cavitation wave to source ejecta mass into the RM unstable sheets at the interface (see [27] for a discussion of cavitation wave ejecta-mass sources). The cavitation wave sources more mass into the RM unstable sheets at the interface boundaries, as compared with the periodic RM unstable sheets between the interfaces whose mass is source is RM unstable bubbles. Further, the size-velocity distributions of the RM unstable sheets at the interfaces are different than those sourced by the bubbles [13].

In the case of the up-finish, the RM unstable dynamics give a better view of the interior sheets without the increased mass- and size-velocity distributions, but the up-finish causes a type of “splash” at the interfaces to unstably grow a low angle. This splash obscures ejecta dynamics near the surface, whereas the down-finish does not.

Our initial PIV and Mie experiments on the DR were done with a large radius, flycut up-finish. But, based on the issues with both finishes, we developed a tailored, down-finish. The tailored finish includes a small number  $N$  of periodic  $\lambda$  with  $h_0$  sandwiched between three perturbations at the edges with  $5\lambda$  with  $h_0$ . Our upcoming Mie and PIV experiments we will field the tailored finish depicted in Fig. 2. We tested this finish on simple evaluation experiments that imply it will give an excellent view of ejecta properties near the surface.

## IR Imaging, LDV, and LN-pin Measurements

Our first single pellet IR-imaging experiments are similar to experiments reported previously in [2], with the exception that our 35 IR experiments were fielded in the improved packages (see Fig. 1) with improved gas- and target-handling. Our vacuum tests are at pressures typically on the order of 0.1 torr and these improved packages often leak at rates  $\ll 0.1$  torr in 5 minutes.

Our first single pellet IR-imaging experiments occurred in December 2017. The 3 mm tall Ce targets were finished with  $\lambda = 100 \mu\text{m}$ ,  $2h_0 = 11 \mu\text{m}$  ( $kh_0 = 0.35$ ), and the 2 mm tall Sn targets were finished with  $\lambda = 40 \mu\text{m}$ ,  $2h_0 = 4 \mu\text{m}$  (in 2017,  $kh_0 = 0.31$ , which we reduced to  $kh_0 = 0.25$  with  $\lambda = 50 \mu\text{m}$  for our finish tests in 2019 and  $\lambda = 100 \mu\text{m}$  on the PIV experiments in 2018); the LN-pins were 23 mm above the surface. Results from those experiments are presently unpublished, but were presented at SCCM-19 in Portland, Oregon.

Velocimetry and LN pin data from six of those experiments are shown in Fig. 3. The left- and center-panels of Fig. 3 (three figures in each panel) are velocimetry data for Sn and Ce ejecta, respectively, transporting in vacuum, and He and  $\text{D}_2$  at initial pressures of  $P_i(\text{He}) = 7086$  torr, and  $P_i(\text{D}_2) = 6080$  torr (our experiments sought to match the post-shock densities of He and  $\text{D}_2$ ). All cases are reaction free with the exception of the lower figure in the central panel of Ce transporting in  $\text{D}_2$ . The right panel shows LN-pin data for the Sn and Ce velocimetry. Clearly seen in the LN-pin and LDV data are differences in drag for Sn and Ce ejecta in otherwise identical conditions. The rates of deceleration are essentially the same for Ce in transporting in He and  $\text{D}_2$ , but the deceleration rates for Sn were much higher than for Ce. Interesting is the time over which the surface velocimetry is seen in the Sn gas experiments,

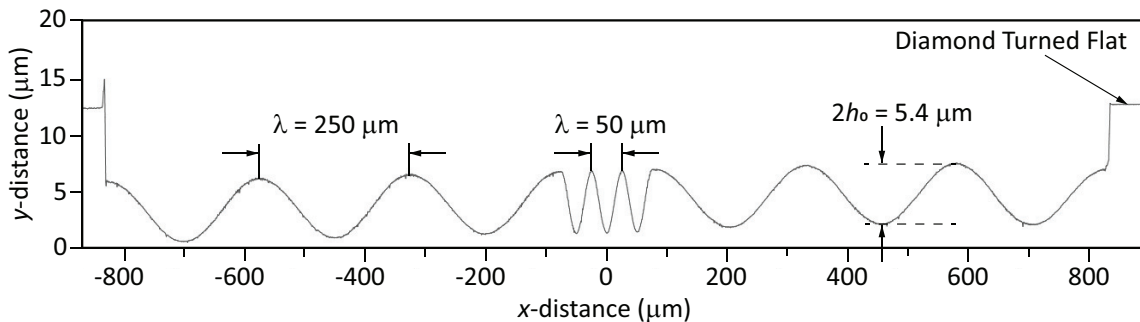


**FIGURE 2.** Test “tailored” finishes for future PIV and Mie experiments. The perturbations will not be offset, as seen in this scan, on our finished targets. Sheet-tip velocities of the outer perturbations will be about 10% of the sheet-tip velocities of the inner perturbations.

as compared with the Ce gas experiments. The Sn surfaces are quickly obscured in He and D<sub>2</sub>, which implies the surface is obscured by the Sn fragments as they breakup into smaller fragments, whereas the Ce surface is seen to much later times. Also note the smooth characteristics of the Sn ejecta pressure profiles, versus that of the Ce ejecta pressure profiles. The Sn are mostly liquid at these loading pressures (in this case,  $u_j(\text{Sn}) \approx 2 \text{ mm}/\mu\text{s}$ , or  $P_L \approx 29 \text{ Gpa}$ ), whereas we have concluded the Ce ejecta are solid, and are therefore not breaking up as rapidly as the Sn.

Our 2017 IR experiments are summarized in Fig. 4. These experiments fielded three IR-cameras on each experiment. When we present six radiance temperatures  $T_R$  for Ce, it is because we fielded two experiments under otherwise identical conditions.

Our thermal models, and even the simple model in [2], explain  $T_R$  for Sn ejecta transporting in He and D<sub>2</sub>, and for Ce transporting in He. In addition, in the absence of reactions, the thermal model predicts that the temperature for Ce transporting in D<sub>2</sub> would equilibrate to around 800 K, implying  $\Delta T \geq 400 \text{ K}$  for Ce transporting in D<sub>2</sub>.

### Coherent Anti-Stokes Raman Spectroscopy

We fielded four single pellet CARS experiments into about 2 atm of D<sub>2</sub> with our improved packages in 2018. The experiments fielded Sn targets with a DT finish to suppress ejecta formation to measure post shock gas temperatures. These were diagnostic development experiments, and represent the first CARS experiments in explosive geometries.

Shot to shot experimental timing varied, but common timing relative to shock breakout at the Sn surface, and Schlieren imaging, implies the data were acquired in the post shock gases at 0.98, 1.12, 2.12 and 2.65 mm beyond the Sn surface at the times after shock breakout (at the surface) that the measurements were made. The CARS diagnostic determined the gas temperatures were  $T_g(D_2) = 504 \pm 100$ ,  $600 \pm 100$ ,  $662 \pm 100$  and  $381 \pm 100 \text{ K}$ , at 0.98, 1.12, 2.12 and 2.65 mm, respectively. The Schlieren images and common timing imply the 2.65 mm measurement was at the interface between the shocked and unshocked gases.

The temperatures make sense. That is, the temperature of the Sn post shock is about 500 K, and at the later times of these measurements the shock velocity is slowing down as the shocked gas decompresses and slips around the target at later times, lowering the gas temperatures over time.

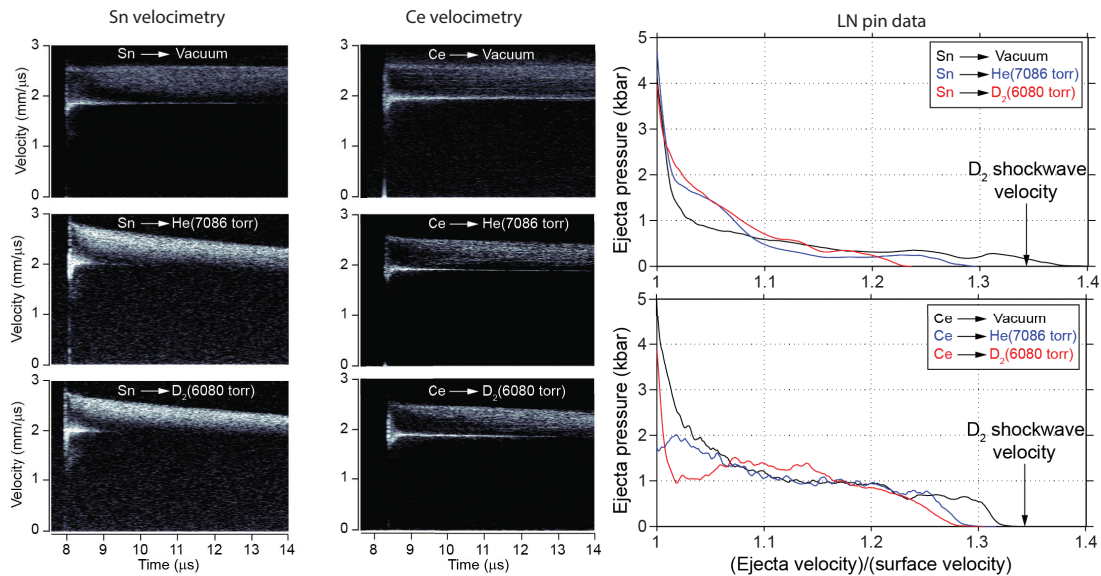


**FIGURE 3.** Typical Sn and Ce velocimetry and Sn LN pin (mass) measurements in vacuum, He and D<sub>2</sub>. The Sn velocimetry are on the left, the Ce velocimetry in the middle, and the LN pin data are on the right.

## Particle Imaging Velocimetry

We fielded six PIV experiments on our “up” finish Sn targets that included 2, 4 or 6 periodic features above the DT background, which invert to form 1, 3 or 5 RM unstable sheets. As this was diagnostic development, we changed the finish on the Sn PIV targets to  $\lambda = 100 \mu\text{m}$ , and  $2h_0 = 8.0 \mu\text{m}$  ( $kh_0 = 0.25$ , and the total ejected areal mass  $\rho_A$  increases by a little more than two, as compared with  $\lambda = 40 \mu\text{m}$  and  $kh_0 = 0.31$ ). The PIV diagnostic is extensively applied on 2 fluid mixing experiments and the approaches are well documented [28]. That said, however, the basic idea is to acquire two high-resolution images near in time, and correlate groups of particles seen in one image with particle groups in the near neighbor image. Such correlations give velocities of the particle groups over time.

In our application, our PIV system included nine doubled Nd:YAG lasers ( $\lambda = 532 \text{ nm}$ ) with 50 mJ pulses of 10 ns duration. As there were nine lasers, the pulses could be emitted on demand, which in our case meant images paired approximately 1, 3, 5, and 7  $\mu\text{s}$  after shockwave breakout at the Sn surface; the companion PIV images were acquired 100 ns later. The ninth laser pulse was acquired on a single high resolution camera (3.4  $\mu\text{m}$  per pixel), and the other 8 laser pulses were acquired on a gated ten frame camera (25.4  $\mu\text{m}$  per pixel). This diagnostic will be important for our ejecta physics experiments going forward.

Figure 5 shows a high-resolution image of a single ejecta sheet acquired with the PIV system, with a magnified region of the same experiment. The images are acquired by scattering from the sheet into the camera system that is aligned normal to the ejecta sheet(s). The laser sheet was aligned with a  $2^\circ$  tilt relative to the perturbations, which means the collected light scatters into the camera system from  $88^\circ$ . The camera resolution is about 25  $\mu\text{m}$ .

We were surprised by the ligament like features in the data. Given the Mie scattering results for Sn transporting in

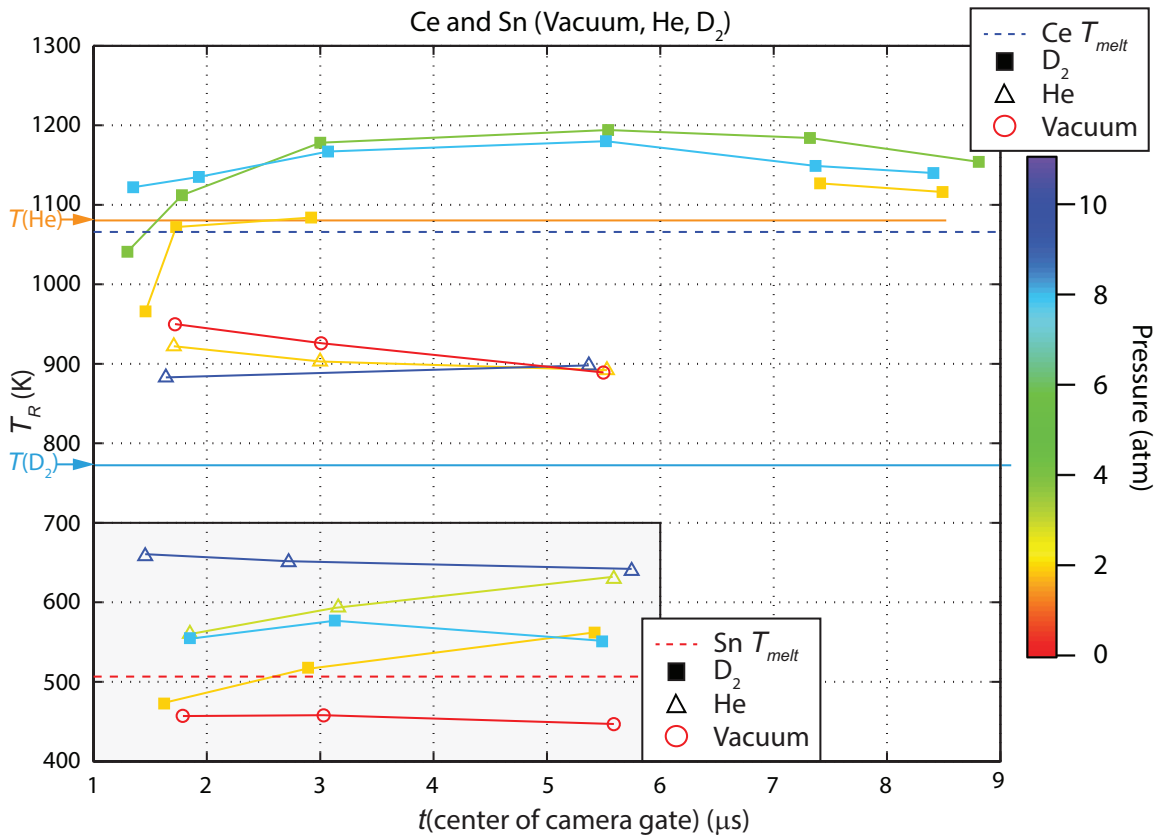


**FIGURE 4.** Radiance measurements for Sn and Ce transporting in vacuum, D<sub>2</sub> and He at different initial gas pressures. Emissivity is assumed to be 1. Calculated post-shock gas temperatures,  $T(\text{He})$  and  $T(\text{D}_2)$  are the same for both Ce and Sn experiments. In Sn temperatures are lower consistent with the melt point, and equilibrate toward temperatures consistent with the gas temperature. In Ce initial temperatures are higher with rapid heating observed in D<sub>2</sub> but not He or vacuum, and final temperatures for D<sub>2</sub> are well above the expected gas temperature.

He, we know the median sizes of ejecta particles are on the order of  $D_m \sim \mathcal{O}(2 \mu\text{m})$ . This means the large imaged spots may include many particles.

We think the periodic ligament features may be caused by chatter (tool vibrations) in the machining processes. Our next experiments will field linear, DT-cut perturbations with the shapes seen in Fig. 2. As seen, the perturbations on these coupons include true sine waves. Given their linear nature, and otherwise DT finish, even in the perturbations, it will be interesting to see whether the tendrill like instabilities observed on the RM unstable sheets will persist.

## Mie Scattering

As noted, the LANL Mie scattering diagnostic as fielded is thoroughly documented in [11, 12, 13], and our recent Mie scattering results on Ce (single PBX 9501 pellet, and 3 mm tall Ce) are reported in these proceedings [26]. All of our Mie scattering data were acquired in the package designs we have published. In the case of the Ce experiments, the packages are so large that that they only support absolute initial  $D_2$  pressures of  $P_i = 1520$  torr, or about 760 torr relative to the local atmospheric pressure.

As noted, our LN-pin and LDV data imply the Ce ejecta include large diameter particles. As we were expecting liquid Ce, and based on our extensive results on liquefied Sn ejecta, we expected small Ce ejecta diameters in He and  $D_2$ . As to liquid Sn ejecta, in vacuum we see median diameters of  $D_m(\text{Sn}, \text{vac}) \approx 1 \mu\text{m}$ , and in He and  $D_2$  up to 1520 torr  $D_m(\text{Sn}, \text{He}) \approx D_m(\text{Sn}, D_2) \approx 2 \mu\text{m}$ . Indeed, on our Ce Mie scattering experiments vacuum we saw  $D_m(\text{Ce}, \text{vac}) \approx 1 \mu\text{m}$ . However, for Ce transporting in He and  $D_2$ , we saw  $D_m(\text{Ce}, \text{He}) \approx D_m(\text{Ce}, D_2) \approx 13 \mu\text{m}$ . Figure 6 shows the Mie scattering results for Ce transporting in vacuum, He and  $D_2$ .

## DISCUSSION

The Mie scattering results surprised us. In He we expected to observe  $D_m(\text{Ce}, \text{He}) \approx D_m(\text{Sn}, \text{He}) \approx 2 \mu\text{m}$ , and for Ce in  $D_2$  we expected  $D_m(\text{Ce}, D_2) \leq D_m(\text{Ce}, \text{He})$ . More surprising was that  $D_m(\text{Ce}, D_2) = D_m(\text{Ce}, \text{He}) \approx 13 \mu\text{m}$ , within uncertainties. Given that the Ce hydride experiences a 30% volume expansion, in spite of the observed minimum  $\Delta T \geq 400$  K the implication was that only a small fraction of the Ce mass had converted to  $\text{CeD}_2$ . From our reactive model, this  $D_m = 13 \mu\text{m}$ , combined with volume in which the Ce ejecta are confined, and with the Ce densities seen

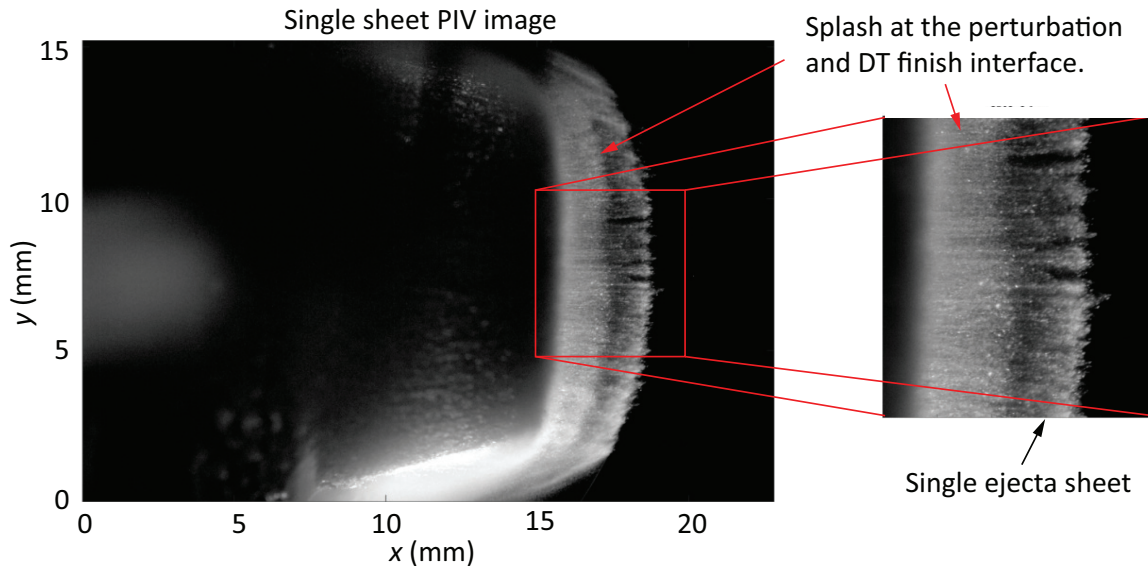


**FIGURE 5.** High resolution PIV image about  $9 \mu\text{s}$  after shockwave breakout at the target surface. These are Sn ejecta transporting in He at initial pressures of  $P_i = 1520$  torr.

in Fig. 3 implies that only about 10% of the Ce ejecta converted to  $\text{CeD}_2$ . Consequently, we could not say rapid breakup was occurring in the presence of reactions.

Importantly, we concluded the Ce ejecta were solid and not liquid. This does not mean that no small fragments formed, but that their scattering signature was overwhelmed by the scattering pattern of the larger diameters. As to why we saw no difference in  $D_m(\text{Ce}, \text{D}_2)$  and  $D_m(\text{Ce}, \text{He})$ ? The post shock temperatures of the Ce and He were similar:  $T(\text{He}) \approx 1100 \text{ K}$ , which means the metal-gas mixture temperatures equilibrate toward the He gas temperature. In addition to this, the Ce,  $\text{CeD}_2$  and  $\text{D}_2$  mixture temperatures were not significantly greater than this. As to why we do not observe the smaller particles? Perhaps they were masked by the splash, where the Mie scattering calculations stop due to multiple scattering effects [26], or perhaps the ejecta particles with  $d > 13 \mu\text{m}$  were breaking up and stabilized at  $D_m = 13 \mu\text{m}$ —the Ce and  $\text{CeD}_2$  are hot, with minimal strength, and their effective viscosities may be stabilizing such that the relative mass at large diameters obscures the scattering pattern from the smaller diameters. The point is we cannot say.

Our fundamental reactive model guides us to expect two outcomes in the presence of reactions, both of which include the generation of heat. In the first case, the  $\text{CeD}_2$  that forms on liquid Ce flakes off of the liquid Ce particles as quickly as it forms, converting a Ce particle of diameter  $d = 1 \mu\text{m}$  to diameters  $d \sim \theta(0.1 \mu\text{m})$  over a timescale of  $1 \mu\text{s}$ —ejecta sizes of this size quickly couple to the gas. In the second case, a  $\text{CeD}_2$  crust grows on the outside of the increasingly hot, liquid Ce core inside the  $\text{CeD}_2$  crust. Nevertheless, we expect the  $\text{CeD}_2$  ejecta to breakup into diameters  $d \sim \theta(0.1 \mu\text{m})$ , but over a timescale of  $t \sim 10 \mu\text{s}$ . Neither of these outcomes were observed, and we were left curious as to where the smaller fragments seen in the vacuum experiment went.

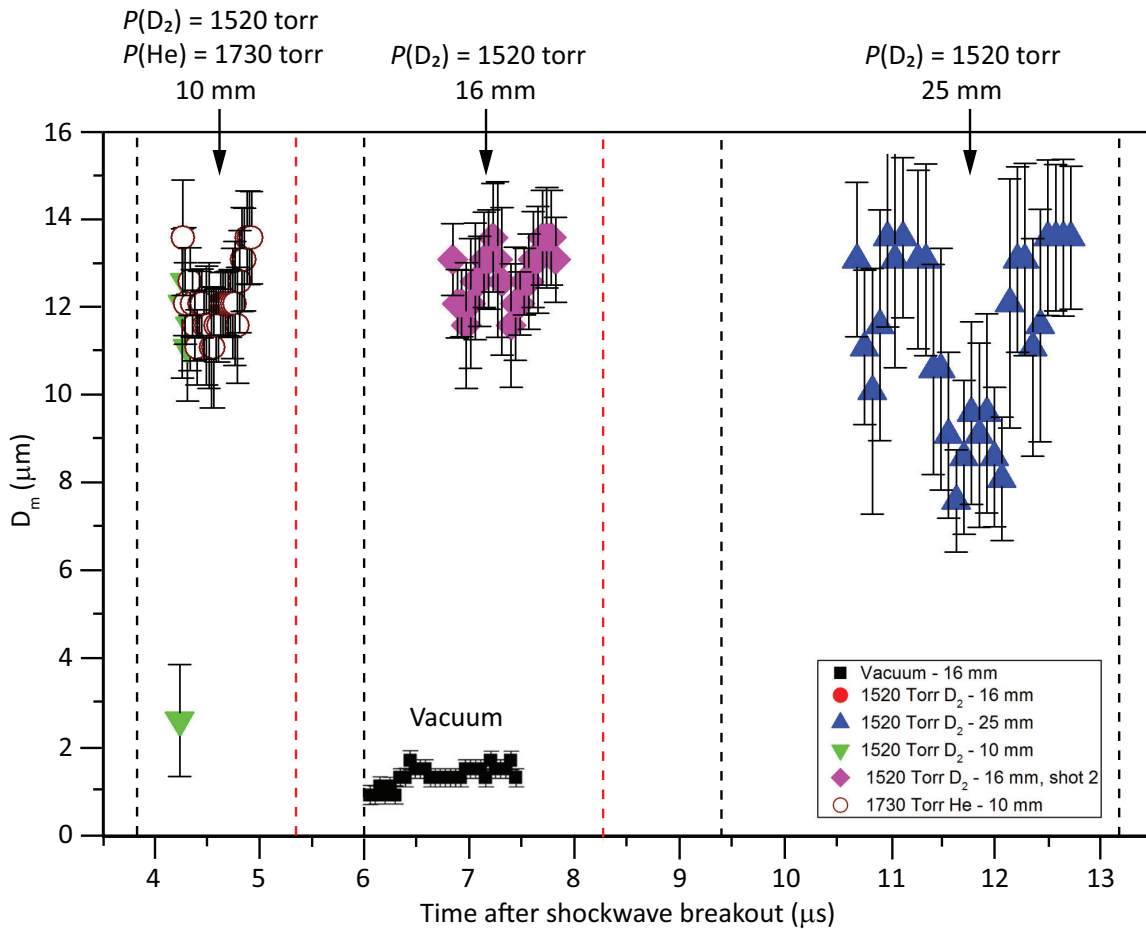


**FIGURE 6.** Median Ce diameters  $D_m$  from the Mie scattering diagnostic in vacuum, He and  $\text{D}_2$ . The diameters for Ce transporting in He are the green triangles, which are mostly obscured by the diameters for Ce transporting in  $\text{D}_2$ .

## Implications

In considering the possibilities for the outcome, we asked what we've missed. In the past, when discussing ejecta sizes we talk about 2 variables: the width  $s$  and  $D_m$  of the scattering distribution. There is a third variable the diagnostic returns,  $G$ , which relates the amplitude of the size distribution defined by the scattering pattern. This amplitude is proportional to the number of particles at the diameters within the distribution with  $D_m$  and  $s$ . We had ascribed meaning to  $D_m$  and  $s$ , but—for us— $G$  was pure *information*. It's not that we were ignorant of  $G$ , but that we are keenly aware that optical sizing diagnostics as applied do not describe partition of ejecta mass (mass- and size-velocity distributions) below the lower resolution limits of the system. That is, we are aware that *Mie scattering predicts the partition of mass above the lower resolution limits of the system*. Thus, unless the Ce ejecta are completely consumed we can say nothing about the size distribution of the fraction of mass that converts from Ce to CeD<sub>2</sub>.

At this point it is important to comment on our lack of use of  $G$ , especially in the context of others who use optical diagnostics to determine sizes and predict the ejected masses [29, 30, 31, 32, 33, 34]. Those who use optical diagnostics in such approaches have either missed or ignored the fact that they can say nothing about the partition of mass below their optical limits.

We were aware that a well calibrated Mie scattering diagnostic measures the size of the mass-distribution that causes the scattering distribution, but we ignored it. That is,  $G$ ,  $D_m$  and  $s$  can be combined with the scattering volume  $V_s$  analytically to equate the ejecta mass that caused the observed scattering patterns. This is important, because the predicted mass can be replaced by the measured mass to constrain the partition of mass below the lower resolution limits of the diagnostic.

## Experimental Changes

Because we concluded the Ce ejecta were solid, we consulted our latest unpublished Ce EOS that we alluded to earlier (private communication with Frank Cherne). This EOS implies we needed to get to 25 GPa, not the 19 GPa as predicted by SESAME 90600. Therefore, we fielded six hydrotests with varying HE and Ce thicknesses. From those experiments, we settled on driving Ce with thickness 1.75 mm with two PBX 9501 pellets. The EOS says we get to 25 GPa in that geometry, and we have fielded IR experiments and measured velocimetry and ejecta since. Those results demonstrate more heating, and we see evidence of rapid breakup. We have not yet studied this geometry with Mie scattering or PIV, but we expect to soon.

## CONCLUSION

We have seen rapid heating of ejecta due to Ce and D<sub>2</sub> reactions, and while we are certain the ejecta—Ce and Sn—are breaking up, we cannot quantify the partition of ejecta mass below the lower resolution limit of our optical diagnostic.

Based on the Mie scattering results, we are aware of no diagnostic as presently applied (including holography, Mie scattering, multiwavelength extinction, microscopy, atomic spectroscopy, etc.) that correctly describes the partition of mass below the lower resolution limits of that diagnostic. Holography can quantify the detected mass by summation, and if total mass is known it quantifies the residual mass below its lower resolution limit, without specifying a size- and mass-velocity distributions. Similarly, the Mie scattering diagnostic returns the mass partition above its lower resolution limit, and the residual mass if the total mass is known. In contrast to holography, however, *the inverted Mie scattering pattern can be constrained with the measured ejecta mass- and velocity-distribution to bound the size, width and amplitude of the ejecta mass partition below the lower resolution limit*.

Specifically, the measured ejecta mass  $m(t)$  from LN-pin and LDV measurements, combined with the measured Mie scattering pattern specifies and constrains the width and size  $\sigma$  and  $\Delta_m$  of  $m(t)$ . That is, the Mie data return  $f(G, s, D_m)$  for the mass with  $d > d_{LRL}$  (LRL = lower resolution limits), whereas the scattering pattern constrained to  $m(t)$  returns  $f(G(m(t)), \sigma, \Delta_m)$ . There is exactly one case where  $f(G, s, D_m) \equiv f(G(m(t)), \sigma, \Delta_m)$ , namely when the diameters of all ejecta have  $d > d_{LRL}$ , which on HE driven (liquid) ejecta experiments never occurs. Therefore, we seek a mass partition that when added to  $f(G, s, D_m)$  returns  $f(G(m(t)), \sigma, \Delta_m)$ . This solution gives an upper bound to the mass partition below the lower limit of the Mie scattering system.

We have done some work in this area with our Mie scattering vacuum data and the ejecta masses we have measured. Using scattering volume geometries, and the Mie equations, we constrained  $G$  with measured ejecta mass and find the

constrained  $G$ :

$$G_c = \frac{6 \bar{\rho}(z, t)}{\pi \rho_0} \exp\left(-\frac{9}{2} w^2\right) \frac{V_s}{D_m^3}, \quad (1)$$

where  $\bar{\rho}$  is the average density in the scattering volume  $V_s$  and  $\rho_0$  is the density of the ejecta. We applied this approach to our Ce vacuum data and find that the constrained solution shifts  $D_m(\text{vac})$  from  $1 \mu\text{m}$  upwards to  $\sim 2 \mu\text{m}$ , and the width doubles as well. Thus, we seek a mass partition that when added to the measured partition gives the constrained partition. *We are exploring this approach.*

## ACKNOWLEDGMENTS

Research presented in this article was supported by the Laboratory Directed Research and Development program of Los Alamos National Laboratory under project number [20070082DR].

## REFERENCES

1. W. T. Buttler, "Understanding ejecta transport, break-up and conversion processes," Tech. Rep. LA-UR-16-23461 (Los Alamos National Laboratory, 2016).
2. W. T. Buttler, S. K. Lamoreaux, R. K. Schulze, J. D. Schwarzkopf, J. C. Cooley, M. Grover, J. E. Hammerberg, B. M. La Lone, A. Llobet, R. Manzanares, J. I. Martinez, D. W. Schmidt, D. G. Sheppard, G. D. Stevens, W. D. Turley, and L. R. Veaser, "Ejecta transport, breakup and conversion," *J. Dynam. Behavior Mater.* **3**, 334–345 (2017).
3. J. D. Schwarzkopf, D. G. Sheppard, J. E. Hammerberg, D. G. Sheppard, R. K. S. J. E. Hammerberg, J. J. G. III, J. C. Cooley, M. Grover, B. M. L. Lone, R. Manzanares, J. I. Martinez, M. M. Schauer, D. W. Schmidt, G. D. Stevens, W. D. Turley, and W. T. Buttler, "Modeling of cerium ejecta in helium and deuterium gases," *Submitted to SCCM-19 AIP Conf. Proc.* (2019).
4. H. Cummins, N. Knable, L. Gampel, and Y. Yeh, "Frequency shifts in light diffracted by ultrasonic waves in liquid media," *Appl. Phys. Lett.* **2**, 62–64 (1963).
5. H. Cummins, N. Knable, L. Gampel, and Y. Yeh, "Spurious harmonic generation in optical heterodyning," *Appl. Opt.* **2**, 823–825 (1963).
6. Y. Yeh and H. A. Cummins, "Localized fluid flow measurements with an HeNe laser spectrometer," *Appl. Phys. Lett.* **4**, 176–178 (1964).
7. J. W. Forman Jr., E. W. George, and R. D. Lewis, "Measurement of localized fluid flow velocities in gases with a laser Doppler flowmeter," *Appl. Phys. Lett.* **7**, 77–78 (1965).
8. W. T. Buttler, S. K. Lamoreaux, F. G. Omenetto, and J. R. Torgerson, "Optical velocimetry," Tech. Rep. LA-UR-04-6453 (Los Alamos National Laboratory, 2004).
9. O. T. Strand, D. R. Goosman, C. Martinez, and T. L. Whitworth, "Compact system for high-speed velocimetry using heterodyne techniques," *Rev. Sci. Instrum.* **77**, 083108 (2006).
10. C. F. McMillan, "Size measurements of high velocity particle distributions," *SPIE* **674**, 289–297 (1986).
11. S. K. Monfared, W. T. Buttler, D. K. Frayer, M. Grover, B. M. LaLone, G. D. Stevens, J. B. Stone, W. D. Turley, and M. M. Schauer, "Ejected particle size measurement using Mie scattering in high explosive driven shockwave experiments," *J. Appl. Phys.* **117**, 223105 (2015).
12. M. M. Schauer, W. T. Buttler, D. K. Frayer, M. Grover, B. M. LaLone, S. K. Monfared, D. S. Sorenson, G. D. Stevens, and W. D. Turley, "Ejected particle size distributions from shocked metal surfaces," *J. Dynam. Behavior Mater.* **3**, 217–224 (2017).
13. M. M. Schauer, W. T. Buttler, D. Sorenson, D. K. Frayer, M. Grover, B. M. LaLone, G. D. Stevens, and W. D. Turley, "Constraining ejecta particle size distributions with light scattering," *AIP Conf. Proc.* **1979**, 080013 (2018).
14. C. S. Speight, L. Harper, and V. S. Smeeton, "Piezoelectric probe for the detection of shock-induced spray and spall," *Rev. Sci. Instrum.* **60**, 3802–3808 (1989).
15. W. S. Vogan, W. W. Anderson, M. Grover, J. E. Hammerberg, N. S. P. King, S. K. Lamoreaux, G. Macrum, K. B. Morley, P. A. Rigg, G. D. Stevens, W. D. Turley, L. R. Veaser, and W. T. Buttler, "Piezoelectric characterization of ejecta from shocked tin surfaces," *J. Appl. Phys.* **98**, 113508 (2005).
16. W. S. Vogan, W. W. Anderson, M. Grover, N. S. P. King, S. K. Lamoreaux, K. B. Morley, P. A. Rigg, G. D. Stevens, W. D. Turley, and W. T. Buttler, "A new spin on an old technology: Piezoelectric ejecta diagnostics for shock environments," *AIP Conf. Proc.* **845**, 1223–1226 (2006).
17. M. B. Zellner, M. Grover, J. E. Hammerberg, R. S. Hixson, A. J. Iverson, G. S. Macrum, K. B. Morley, A. W. Obst, R. T. Olson, J. R. Payton, P. A. Rigg, N. Routley, G. D. Stevens, W. D. Turley, L. Veaser, and W. T. Buttler, "Effects of shock-breakout pressure on ejection of micron-scale material from shocked tin surfaces," *J. Appl. Phys.* **102**, 013522 (2007).
18. M. B. Zellner, M. Grover, J. E. Hammerberg, R. S. Hixson, A. J. Iverson, G. S. Macrum, K. B. Morley, A. W. Obst, R. T. Olson, J. R. Payton, P. A. Rigg, N. Routley, G. D. Stevens, W. D. Turley, L. Veaser, and W. T. Buttler, "Erratum: 'Effects of shock breakout pressure on ejection of micron scale material from shocked tin surfaces' [*J. Appl. Phys.* **102**, 013522 (2007)];" *J. Appl. Phys.* **103**, 109901 (2008).
19. M. B. Zellner, W. Vogan-McNeil, G. T. Gray III, D. C. Huerta, N. S. P. King, G. E. Neal, S. J. Valentine, J. R. Payton, J. Rubin, G. D. Stevens, W. D. Turley, and W. T. Buttler, "Surface preparation methods to enhance dynamic surface property measurements of shocked metal surfaces," *J. Appl. Phys.* **103**, 083521 (2008).
20. M. B. Zellner, W. Vogan-McNeil, J. E. Hammerberg, R. S. Hixson, A. W. Obst, R. T. Olson, J. R. Payton, P. A. Rigg, N. Routley, G. D. Stevens, W. D. Turley, L. Veaser, and W. T. Buttler, "Probing the underlying physics of ejecta production from shocked Sn samples," *J. Appl. Phys.* **103**, 123502 (2008).

21. M. B. Zellner and W. T. Buttler, "Exploring Richtmyer-Meshkov instability phenomena and ejecta cloud physics," *Appl. Phys. Lett.* **93**, 114102 (2008).
22. M. B. Zellner, M. Byers, J. E. Hammerberg, T. C. Germann, G. Dimonte, P. A. Rigg, G. D. Stevens, W. D. Turley, and W. T. Buttler, "Influence of shockwave profile on ejection of micron-scale material from shocked sn surfaces: An experimental study," *DYMAT - International Conference on the Mechanical and Physical Behaviour of Materials under Dynamic Loading* **1**, 89–94 (2009).
23. M. B. Zellner, G. Dimonte, T. C. Germann, J. E. Hammerberg, P. A. Rigg, Stevens, W. D. Turley, and W. T. Buttler, "Influence of shockwave profile on ejecta," *Shock Compression of Condensed Matter-2009, AIP Conf. Proc.* **1195**, 1047–1050 (2009).
24. B. J. Jensen, F. J. Cherne, J. C. Cooley, M. V. Zhernokletov, and A. E. Kovalev, "Shock melting of cerium," *Phys. Rev. B* **81**, 214109 (2010).
25. C. W. Greeff and S. Crockett, "A Sesame equation of state for dense Ce," Tech. Rep. LA-UR-16-21738 (Los Alamos National Laboratory, 2017).
26. M. M. Schauer, R. Manzanares, J. I. Martinez, D. W. Schmidt, M. Grover, G. D. Stevens, W. D. Turley, and W. T. Buttler, "Ejected particle size distributions from shocked cerium targets," *Submitted to SCCM-19 AIP Conf. Proc.* (2019).
27. W. T. Buttler, D. Renner, C. Morris, R. Manzanares, E. K. Anderson, J. J. G. III, J. Heidemann, R. M. Kalas, A. Llobet, J. I. Martinez, P. V. M. Jr., J. R. Payton, A. Saunders, D. W. Schmidt, A. M. Tainter, D. Tupa, S. W. Vincent, and W. Vogan-McNeil, "Cavitation bubble interacting with a richtmyer-meshkov unstable sheet and spike," (Amer. Inst. Phys., Melville, NY, 2018) p. 080003.
28. R. J. Adrian and J. Westerweel, *Particle Image Velocimetry* (Cambridge University Press, New York, 2010).
29. G. Prudhomme, P. Mercier, L. Berthe, J. Bénier, and P.-A. Frugier, "Frontal and tilted PDV probes for measuring velocity history of laser-shock induced calibrated particles," *J. Phys. Conf. Ser.* **500**, 142022 (2014).
30. G. Prudhomme, P. Mercier, and L. Berthe, "PDV experiments on shock-loaded particles," *J. Phys. Conf. Ser.* **500**, 142027 (2014).
31. V. A. Ogorodnikov, A. L. Mikhailov, V. S. Sasik, S. V. Erunov, M. A. Syrunin, A. V. Fedorov, N. V. Nevmerzhitskii, E. V. Kulakov, O. A. Kleshchevnikov, M. V. Antipov, I. V. Yurtov, A. V. Rudnev, A. V. Chapaev, A. S. Pupkov, E. D. Senkovskii, E. A. Sotskov, V. V. Glushikhin, I. A. Kalashnik, S. A. Finyushin, E. A. Chudakov, and D. A. Kalashnikov, "Effect of a gas on the ejection of particles from the free surface of a sample subjected to a shock wave with various intensities," *J. Exper. Theoretical Phys.* **123**, 357–362 (2016).
32. P. T. Steele, B. A. Jacoby, S. M. Compton, and J. O. Sinibaldi, "Advances in ejecta diagnostics at LLNL," *J. Dynam. Behavior Mater.* **3**, 253–264 (2017).
33. J.-E. Franzkowiak, G. Prudhomme, P. Mercier, S. Lauriot, E. Dubreuil, and L. Berthe, "PDV-based estimation of ejecta particles' mass-velocity function from shock-loaded tin experiment," *Rev. Sci. Instrum.* **89**, 033901 (2018).
34. A. V. Andriyash, M. V. Astashkin, V. K. Baranov, A. G. Golubinskii, D. A. Irinichev, V. Y. Khatunkin, A. N. Kondratev, S. E. Kuratov, V. A. Mazanov, D. B. Rogozkin, and S. N. Stepushkin, "Application of photon doppler velocimetry for characterization of ejecta from shock-loaded samples," *J. Appl. Phys.* **123**, 243102 (2018).